

## ARTICLE OPEN



# Mice with deficiency in *Pcdh15*, a gene associated with bipolar disorders, exhibit significantly elevated diurnal amplitudes of locomotion and body temperature

Daisuke Mori <sup>1,2,3,16</sup>✉, Chihiro Inami<sup>4,5,16</sup>, Ryosuke Ikeda<sup>1</sup>, Masahito Sawahata<sup>4</sup>, Shinji Urata<sup>6,7</sup>, Sho T. Yamaguchi<sup>5</sup>, Yohei Kobayashi<sup>8</sup>, Kosuke Fujita<sup>9</sup>, Yuko Arioka <sup>3,10</sup>, Hiroki Okumura<sup>3,4</sup>, Itaru Kushima <sup>1,3,11</sup>, Akiko Kodama<sup>1,3</sup>, Toshiaki Suzuki <sup>1</sup>, Takashi Hirao<sup>1</sup>, Akira Yoshimi <sup>12</sup>, Akira Sobue<sup>4</sup>, Takahiro Ito<sup>12</sup>, Yukikiro Noda<sup>12</sup>, Hiroyuki Mizoguchi<sup>4</sup>, Taku Nagai <sup>4,13</sup>, Kozo Kaibuchi<sup>14</sup>, Shigeo Okabe <sup>7</sup>, Koji Nishiguchi<sup>9</sup>, Kazuhiko Kume <sup>5</sup>, Kiyofumi Yamada<sup>4</sup> and Norio Ozaki <sup>3,15</sup>

© The Author(s) 2024

Genetic factors significantly affect the pathogenesis of psychiatric disorders. However, the specific pathogenic mechanisms underlying these effects are not fully understood. Recent extensive genomic studies have implicated the protocadherin-related 15 (*PCDH15*) gene in the onset of psychiatric disorders, such as bipolar disorder (BD). To further investigate the pathogenesis of these psychiatric disorders, we developed a mouse model lacking *Pcdh15*. Notably, although *PCDH15* is primarily identified as the causative gene of Usher syndrome, which presents with visual and auditory impairments, our mice with *Pcdh15* homozygous deletion (*Pcdh15*-null) did not exhibit observable structural abnormalities in either the retina or the inner ear. The *Pcdh15*-null mice showed very high levels of spontaneous motor activity which was too disturbed to perform standard behavioral testing. However, the *Pcdh15* heterozygous deletion mice (*Pcdh15*-het) exhibited enhanced spontaneous locomotor activity, reduced prepulse inhibition, and diminished cliff avoidance behavior. These observations agreed with the symptoms observed in patients with various psychiatric disorders and several mouse models of psychiatric diseases. Specifically, the hyperactivity may mirror the manic episodes in BD. To obtain a more physiological, long-term quantification of the hyperactive phenotype, we implanted nano tag<sup>®</sup> sensor chips in the animals, to enable the continuous monitoring of both activity and body temperature. During the light-off period, *Pcdh15*-null exhibited elevated activity and body temperature compared with wild-type (WT) mice. However, we observed a decreased body temperature during the light-on period. Comprehensive brain activity was visualized using c-Fos mapping, which was assessed during the activity and temperature peak and trough. There was a stark contrast between the distribution of c-Fos expression in *Pcdh15*-null and WT brains during both the light-on and light-off periods. These results provide valuable insights into the neural basis of the behavioral and thermal characteristics of *Pcdh15*-deletion mice. Therefore, *Pcdh15*-deletion mice can be a novel model for BD with mania and other psychiatric disorders, with a strong genetic component that satisfies both construct and surface validity.

*Translational Psychiatry* (2024)14:216; <https://doi.org/10.1038/s41398-024-02952-6>

## INTRODUCTION

Extensive epidemiological research, including twin-, adoption-, family-, and population-based studies of increasing quality, has consistently demonstrated significant heritability in all major psychiatric disorders [1]. This evidence suggests that genetic factors are pivotal in predisposing individuals to these conditions. Consequently, genomic studies have been constantly emphasized

to elucidate the intricate pathogenic mechanisms associated with these disorders.

Recent genomic investigations have highlighted the protocadherin related 15 (*PCDH15*) gene as a potential key player in the etiology of psychiatric ailments. The relationship between *PCDH15* and the disorders is striking for several reasons. Georgieva et al. genotyped 368 bipolar disorder (BD) and 76 schizophrenia (SCZ)

<sup>1</sup>Department of Psychiatry, Nagoya University Graduate School of Medicine, Nagoya, Japan. <sup>2</sup>Brain and Mind Research Center, Nagoya University, Nagoya, Aichi, Japan. <sup>3</sup>Department of Pathophysiology of Mental Disorders, Nagoya University Graduate School of Medicine, Nagoya, Aichi, Japan. <sup>4</sup>Department of Neuropsychopharmacology and Hospital Pharmacy, Nagoya University, Graduate School of Medicine, Nagoya, Aichi, Japan. <sup>5</sup>Department of Neuropharmacology, Graduate School of Pharmaceutical Sciences, Nagoya City University, Nagoya, Aichi, Japan. <sup>6</sup>Department of Otolaryngology, Graduate School of Medicine, The University of Tokyo, Tokyo Pref., Japan. <sup>7</sup>Department of Cellular Neurobiology, Graduate School of Medicine, The University of Tokyo, Tokyo Pref., Japan. <sup>8</sup>Sumitomo Pharma Co., Ltd., Osaka City, Osaka Pref., Japan. <sup>9</sup>Department of Ophthalmology, Nagoya University Graduate School of Medicine, Nagoya, Aichi, Japan. <sup>10</sup>Center for Advanced Medicine and Clinical Research, Nagoya University Hospital, Nagoya, Aichi, Japan. <sup>11</sup>Medical Genomics Center, Nagoya University Hospital, Nagoya, Aichi, Japan. <sup>12</sup>Division of Clinical Sciences and Neuropsychopharmacology, Meijo University Faculty of Pharmacy, Nagoya, Aichi, Japan. <sup>13</sup>Division of Behavioral Neuropharmacology, International Center for Brain Science (ICBS), Fujita Health University, Toyoake, Aichi, Japan. <sup>14</sup>Division of Cell Biology, International Center for Brain Science, Fujita Health University, Toyoake, Aichi, Japan. <sup>15</sup>Institute for Glyco-core Research (iGCORE), Nagoya University, Nagoya, Aichi, Japan. <sup>16</sup>These authors contributed equally: Daisuke Mori, Chihiro Inami. ✉email: d-mori@med.nagoya-u.ac.jp

Received: 29 December 2023 Revised: 16 May 2024 Accepted: 20 May 2024

Published online: 28 May 2024

probands, along with their parents. They identified and validated 21 de novo copy number variants (CNVs), including a *PCDH15* deletion in one patient with BD [2]. Another CNV analysis also confirmed *PCDH15* deletions in patients with BD [3]. Our cross-disorder analysis of genic and regulatory CNVs in BD, SCZ, and autism spectrum disorder (ASD) identified *PCDH15* variants in five, one, and two patients, respectively, establishing a link between *PCDH15* deletion and BD pathogenesis [4]. Additionally, cadherin23 (CDH23), which interacts with *PCDH15* in their extracellular domains [5], has been linked to SCZ and attention deficit hyperactivity disorder [6–8]. Nevertheless, the precise implications of this protein–protein interaction in neural contexts remain elusive, and the molecular pathogenesis of *PCDH15* in neurological states is yet to be thoroughly explored. Notably, when induced into glutamatergic and GABAergic neurons, induced pluripotent stem cells from patients with BD and a *PCDH15* deletion exhibited both dendritic shortening and a decline in synapse numbers [9].

As a cadherin superfamily member, *PCDH15* contributes to neural differentiation and synapse formation [6]. Both the Human Protein Atlas database and the Allen Mouse Brain Atlas indicate widespread *PCDH15* expression in brain regions, such as the cortex, midbrain, cerebellum, and hippocampus, across humans and mice. *PCDH15* is highly expressed in human oligodendrocyte progenitor cells. Moreover, it is crucial for their proliferation and significantly influences white matter development and myelination [10]. Consequently, *PCDH15* is indispensable in brain neurons and glial cells.

*PCDH15* forms tip-link filaments in sensory hair cells. It is also associated with Usher syndrome type 1 (USH1) [11], the most severe Usher syndrome subtype because of its symptoms such as profound hearing loss, lack of vestibular response, and early-onset retinitis pigmentosa [12, 13]. Notably, there are several reported cases of Usher syndrome in patients presenting with coexisting psychiatric disorders such as BD [14, 15]. However, most Usher syndrome research primarily focuses on retinal and inner ear pathologies, overlooking potential brain pathologies. Unsurprisingly, there is limited knowledge of the relationship between the pathogenesis of BD and other psychiatric disorders and their relationship with *PCDH15*.

Animal models, such as the *Pcdh15*-deletion mice, are crucial for understanding the genetic factors responsible for the development of psychiatric disorders. In the evaluation of animal models for psychiatric disorders, researchers typically consider the following three criteria: (1) surface validity, which reflects the similarities in behavioral features between the animal model and the corresponding human disorder; (2) predictive validity, which assesses the degree to which effective treatments in humans produce similar effects in the model; and (3) construct validity, which considers whether a shared mechanistic theory can explain the animal model and its corresponding human disorder [16–18]. However, despite the abundant animal models developed for psychiatric disorders, few have successfully met multiple validity criteria [19–22].

In this study, we evaluated the behavioral phenotype of *Pcdh15*-deletion mice to establish face validity, ensuring the appropriateness of the model for investigating the mechanisms linking *Pcdh15* deletion to psychiatric disorders such as BD. Additionally, we examined the neural underpinnings of these behavioral traits using whole-brain c-Fos mapping.

## MATERIALS AND METHODS

### Animal experiments

All research and animal care procedures were ethically approved by the Nagoya University Animal Care and Use Committee. Mice were housed in groups of up to six animals per cage and were maintained under a standard 12-h light/dark cycle (light period: 9:00–21:00) at a constant temperature of 23 °C. Food and water were provided ad libitum.

### Generation of *Pcdh15*-deletion mice

*Pcdh15*-deletion mice were generated using the CRISPR/Cas9 method as previously described [23–26]. Guide RNAs were designed to target exon 5 (NM\_001142746.1) of the mouse *Pcdh15* gene. For detailed information, refer to the supplementary material.

### Histological analysis of the inner ear and retina of *Pcdh15*-deletion mice

The inner ear of newborn *Pcdh15*-null was isolated, and cochlear morphology was assessed by staining with a myosin (Myo7A) antibody [27]. Rhodamine phalloidin was used for labeling F-actin. The retinas from 8-week-old *Pcdh15*-deletion mice were isolated, and retinal morphology was evaluated via staining with peanut agglutinin (PNA) or Reversin antibody [28].

### General behavioral analysis

General behavioral analysis of *Pcdh15*-het followed previously established protocols [24, 25] and commenced with the open field test at 8 weeks of age. A series of tests were conducted on 15 male WT and 15 male *Pcdh15*-het. Data are presented as mean ± standard error. Statistical comparisons between two groups were performed using a two-tailed Student's t-test. Differences in cliff avoidance reactions were assessed using the Chi-square test [29]. For locomotor activity, PPI test, fear conditioning test, and rota-rod test, repeated analysis of variance (ANOVA) was applied. Multiple group comparisons were analyzed using one-way ANOVA, followed by Tukey's test when F ratios reached significance ( $p < 0.05$ ). Further details can be found in the Supplementary Materials.

### Measurement of activity and body temperature using a small sensor chip: nano tag

The nano tag (Kissei Comtec Co. Ltd., Nagano, Japan), a device measuring spontaneous locomotive activities and body temperature, was surgically implanted into the abdominal cavity of mice. After surgery, mice were allowed ten days to recover and acclimate to the light–dark cycle. Groups of five mice were housed together in a single cage, with bedding changes and provision of food and water once a week during the light phase. Locomotor activity and body temperature were recorded every 5 min over a continuous 6-week period. Analysis of locomotor activity and body temperature was performed using the nano tag Viewer software (Kissei Comtec Co., Ltd.).

### Mapping of mouse brain activity through automated volume analysis of c-Fos

The analyses aimed to accurately detect, locate, and quantify neuronal activity across the entire brain of the model mice. Each set consisted of three male *Pcdh15*-null at 15 weeks of age and three male WT. Following at least 1 week of synchronization with the light–dark cycle, perfusion fixation was performed at ZT7 or ZT13 using 4% paraformaldehyde/PBS (-). The samples were sent to Certerra Co. Ltd. (USA) for c-Fos expression profiling via immunostaining and light-sheet fluorescence imaging. Automated mapping was conducted using the open-source software ClearMap [30].

For additional materials and methods, please refer to the Supplementary Materials section.

## RESULTS

### Generation of *Pcdh15*-deletion mice

To elucidate the phenotypic abnormalities associated with the onset of mental disorders observed in *PCDH15*-deletion subjects, we employed CRISPR–Cas9 (clustered regularly interspaced short palindromic repeats and CRISPR-associated protein 9) genome editing technique to generate a genetically modified mouse model (Fig. 1a) [26]. The conservation of the *Pcdh15* gene structure between humans and mice has been well established [31]. Leveraging this fact, we designed CRISPR-targeted guide RNAs and single-stranded DNA to facilitate the insertion of a FLAG-tag sequence and a stop codon into exon 5, thus creating the *Pcdh15*-deletion model mouse (Fig. 1a and S1a). The #1 guide RNA was chemically synthesized as a CRISPR RNA, and transactivating CRISPR RNA (tracr-RNA), Cas9 protein, and donor DNA

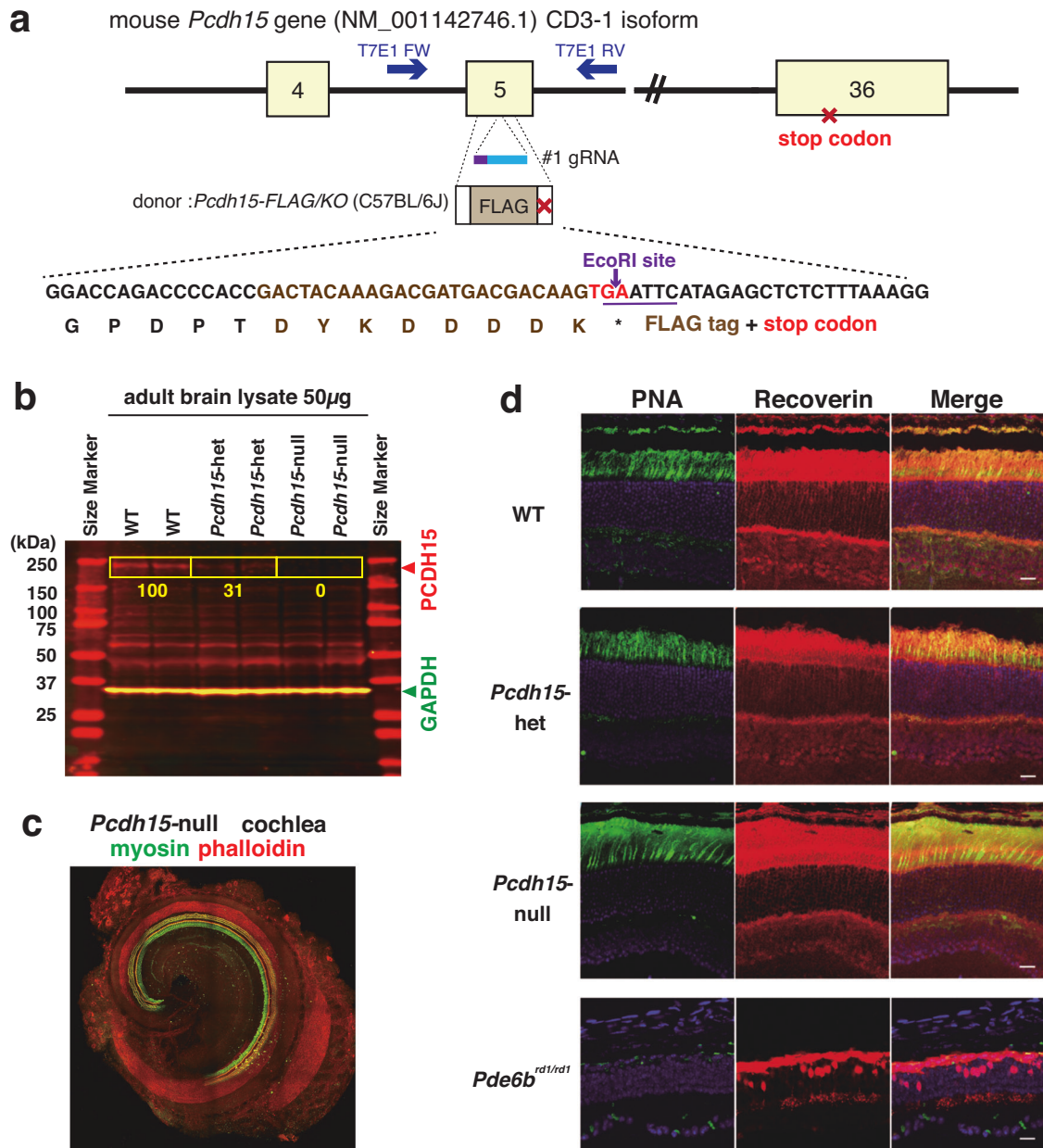


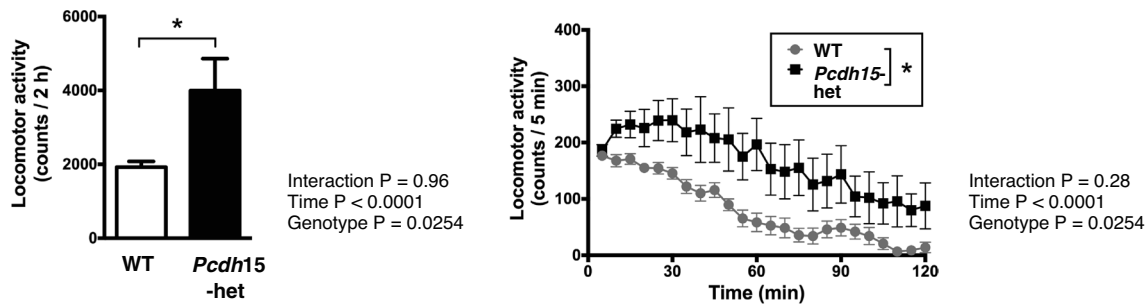
**Fig. 1** Generation of *Pcdh15*-deletion model mice by the CRISPR–Cas9 system. **a** Schematic representation illustrating the strategy employed for deleting the mouse *Pcdh15* gene using the CRISPR–Cas9 system. The CRISPR–Cas9 knock-in approach aimed to insert a FLAG tag and a stop codon into the *Mus musculus Pcdh15* (NCBI: NM\_001142746.1, 9150 bp mRNA) exon 5 (594–754). A specific *EcoRI* digestion site was introduced solely in the mutant allele to enable genotyping through polymerase chain reaction. **b** Immunoblotting analysis confirming the deletion of full-length PCDH15 in the brains of *Pcdh15*-deletion mice. Each lane contains 50 µg of whole-brain extracts from adult WT, *Pcdh15*-het, and *Pcdh15*-null. Signal detection and quantification were performed using the Odyssey system by LI-COR Biosciences (Lincoln, Nebraska, US). The calculated molecular weight of the PCDH15 CD3 isoform is approximately 183 kDa, denoted by the red signal. The green signal represents the internal control GAPDH. **c** Confocal microscope image showing the structure of the inner ear in *Pcdh15*-null immediately after birth. Myosin (green) and phalloidin (red) co-staining reveals the cochlear morphology. **d** Immunohistochemical staining of the retina from *Pcdh15*-null. Retinas from 4-week-old *Pcdh15*-null, *Pcdh15*-het, and WT were stained with peanut agglutinin (PNA; green) and Recoverin (red). Normal formation of the photoreceptor and bipolar cell layers is observed in all genotypes, compared with *Pde6b*<sup>rd1/rd1</sup> mice that display retinal degeneration [28]. *Pcdh15* protocadherin related 15, *Pcdh15*-het *Pcdh15* heterozygous deletion mice, *Pcdh15*-null *Pcdh15* homozygous deletion mice, WT wild-type mice.

were co-microinjected into 121 fertilized eggs in C57BL/6J mice breeding in Charles River Inc (Wilmington, Massachusetts, US) and cultured until the two-cell stage. Of these eggs, 75 were subsequently transplanted into the oviducts of pseudopregnant mice, resulting in the birth of 19 littermates. Ultimately, through polymerase chain reaction cloning, the successful generation of two knock-in mice was confirmed according to the design (Fig.

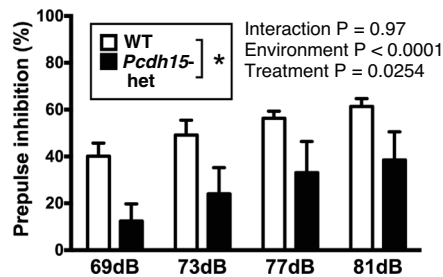
S1b). For conventional genotype screening of the model mice, primers were meticulously designed to distinguish between wild-type mice (WT) and mutant (Flag-KO) alleles via agarose gel electrophoresis (Fig. S1c).

Immunoblot analysis was performed to validate the protein expression level of PCDH15 in the newly generated *Pcdh15*-deletion mice (Fig. 1b). In the adult brain, PCDH15 expression in

### a Locomotor activity test



### b Prepulse inhibition test



### c Cliff avoidance test

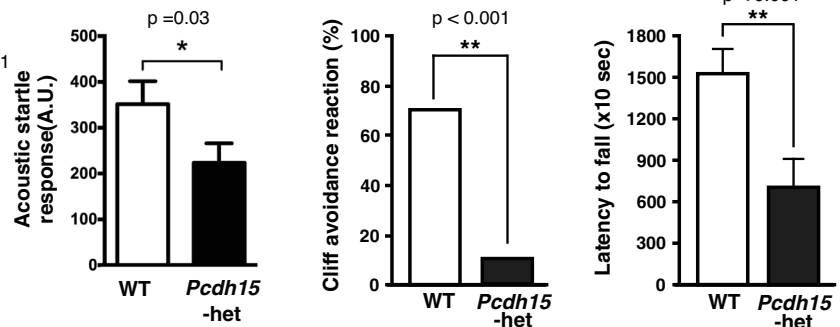


**Fig. 2 Behavioral analyses of *Pcdh15*-het.** **a** Locomotor activity test results depicting total activity during a 2-h measurement period (left), and activity recorded every 5 min (right). **b** Results of the prepulse inhibition (PPI) test.  $n = 15$  for male WT mice,  $n = 15$  for male *Pcdh15*-het in panels a and b. The data of locomotor activity test and PPI were analyzed using a two-way ANOVA. **c** Cliff avoidance test outcomes illustrating the percentage of cliff avoidance reaction (left) and the latency of falling from a cliff (right).  $n = 14$  for male WT,  $n = 14$  for male *Pcdh15*-het in panel 2c. Data are presented as the mean  $\pm$  standard error of the mean (SEM). Student's *t*-test was used for these analyses. \*\* $p < 0.01$ ; \* $p < 0.05$  indicate statistical significance. For additional information, please refer to Table 1.

*Pcdh15*-het was 31% of that measured in WT, whereas PCDH15 was scarcely detectable in *Pcdh15*-null. Employing the PCDH15-specific antibody, immunoblotting on major organs of WT revealed discernible signals solely in the brain (Fig. S1d). Furthermore, the presence of PCDH15 protein was evident in the brain throughout developmental stages into adulthood, with a clear peak during the initial 3 days after birth (Fig. S1e). In the *Pcdh15*-null allele, because of the study design, FLAG tags were added in frame. Attempts were made to confirm the presence or absence of a truncated FLAG protein using immunoblotting; however, it could not be detected with the widely used anti-FLAG antibody (M2 mouse monoclonal antibody, Sigma-Aldrich, US) (data not shown). Within primary cultured neurons, the expression of PCDH15 protein increased as the neurons matured (Fig. S1f). *Pcdh15*-null exhibited normal birth and growth patterns. Detailed examination of their brains revealed the absence of significant structural anomalies (Fig. S1g). Considering that retinal and inner ear structural abnormalities have been reported in spontaneously occurring *Pcdh15*-deletion mice [32], we meticulously examined the pathology of our *Pcdh15*-null and found normal structural features (Figs. 1c and d).

#### General behavioral analysis of *Pcdh15*-het

*Pcdh15*-null displayed marked hyperactivity (Movie S1). Consequently, comprehensive behavioral assessments were exclusively conducted on *Pcdh15*-het, which exhibited elevated locomotor activity and reduced prepulse inhibition (PPI) (Figs. 2a, b, and S2; Table 1). Additionally, in the cliff avoidance test, a metric for assessing impulsivity, *Pcdh15*-het spent significantly shorter time to jump off the platform and exhibited an absence of cliff avoidance response (Fig. 2c). There were no significant changes observed between WT and *Pcdh15*-het (Fig S2 and Table 1) in the

open field, Y-maze, elevated cross maze, rotarod, novel object recognition test, social interaction, and fear conditioning test.

#### Elevated locomotion and body temperature amplitudes in *Pcdh15*-null

We focused on the hyperactivity of *Pcdh15*-deficient mice. In a 24-h locomotor activity test conducted on *Pcdh15*-WT, *Pcdh15*-het, and *Pcdh15*-null mice, the *Pcdh15*-null mice exhibited intense activity during the dark phase (Fig. S3). Moreover, to observe the characteristics of *Pcdh15*-deletion mice under more physiologically relevant conditions, we conducted continuous measurements of spontaneous locomotion and body temperature in both *Pcdh15*-null and WT. Thus, we introduced a small accelerometer chip (nano tag<sup>®</sup>) into the abdominal cavity of each mouse. One week after implantation, the mice were allowed to acclimate to an environment with alternating light-on/off periods set at Zeitgeber time 0 (ZT0) (9:00) and ZT12 (21:00) for an additional week. Thereafter, the measurement phase commenced.

The activity profiles distinctly revealed the nocturnal nature of both mouse groups, with *Pcdh15*-null exhibiting substantially higher levels of activity (Figs. 3a, b, S4a, and b). Mesh plots were generated for time, activity and body temperature, and days over the course of 6 weeks of continuous monitoring (Figs. 3c–f). The pronounced surge in activity during the light-off period in *Pcdh15*-null remained statistically significant across the entire duration of measurement (Figs. 3c, d, g, S4c, and d). These data also include activity noise generated by weekly changes in bedding. In terms of body temperature, the difference between the highest and lowest body temperature within a single day for *Pcdh15*-null was 1.77 times greater than that of WT (WT: 1.736 °C; *Pcdh15*-null: 3.072 °C; Fig. 3h, S4e, and f).

Furthermore, analysis of the temporal patterns showed that both WT and *Pcdh15*-null exhibited their lowest body temperature

**Table 1.** Comparison of behavioral changes between WT mice and the *Pcdh15* heterozygous deletion mutant in each test.

Test	parameter	Result
Open-field test	Inner zone (time) :	ND
	Outer zone (time) :	ND
Elevated plus maze test	Open arm (time) :	ND
	Closed arm (time) :	ND
	Open arm (counts) :	ND
	Closed arm (counts) :	ND
Light dark transition test	Total (counts) :	ND
	Light box (time) :	ND
	Dark box (time) :	ND
Y-maze test	Alternation behavior (%) :	ND
	Total arm entry:	ND
Novel object recognition test	Exploratory preference (%) :	ND
	Total exploratory time :	ND
Fear conditioning test	Training (time) :	ND
	Contextual (time) :	ND
	Cue (time) :	ND
Rota-rod test	Training (time)	ND
	Test (time)	ND
Locomotor activity test	Locomotor activity (time course) :	↑
Social interaction test	Habituation (empty) :	ND
	1st session (stranger 1) :	ND
	2nd session (stranger 1 + 2) :	ND
Prepulse inhibition test	PPI (%) :	↓
	Startle response :	↓
Cliff avoidance test	Cliff avoidance reaction (%) :	↓
	Latency to fall (x10 sec) :	↓

Behavioral tests were performed using 15 male WT mice and 15 male *Pcdh15*-het mice. All data are reported as the mean  $\pm$  standard error of the mean (SEM) and were analyzed using the Prism software. The data from three-chambered social-interaction, PPI, locomotor, rota-rod, elevated plus maze, novel object recognition, and fear-conditioning tests were analyzed using the two-way ANOVA with or without repeated measures, followed the post-hoc Bonferroni test. The data obtained for PPI (Acoustic startle response), locomotor (Locomotor activity), rota-rod (Test phase), open field, Y-maze, and fear-conditioning (contextual) parameters were assessed using the Mann–Whitney *U* test.

↑: higher than the WT, ↓: lower than the WT, ND: no difference

around ZT7 (16:00) and their highest body temperature around ZT13 (22:00). These patterns were consistently observed throughout the entire monitoring period (Figs. 3e, f, h, S4e, and f). *Pcdh15*-null did not show significant circadian anomalies (Fig. S5a). Their daily rest duration remained consistent with that of the WT, despite their elevated activity levels (Figs. S5b and c).

### c-Fos mapping in *Pcdh15*-null whole brain

To elucidate the underlying neural circuitry responsible for the behavioral phenotypes and distinctive diurnal temperature fluctuations in *Pcdh15*-deletion mice, we thoroughly investigated the variations in expression levels of neural activity markers across the entire brain of both WT and *Pcdh15*-null using c-Fos mapping at two specific time points, namely light-off and light-on [33, 34].

At ZT7 or ZT13, we conducted perfusion and fixation procedures for both WT and *Pcdh15*-null, followed by brain removal and transparency enhancement to facilitate whole-brain c-Fos mapping [35]. During ZT13, *Pcdh15*-null exhibited areas of elevated and diminished c-Fos expression compared with those of WT (Fig. 4a and b). Notably, the regions displaying elevated c-Fos expression during ZT13 in *Pcdh15*-null were primarily situated in the cortex, encompassing specific areas such as the primary somatosensory region, secondary motor regions, and primary visual region (Fig. S6a). Conversely, at ZT7, there was a significant reduction in c-Fos expression across the entire cortex in *Pcdh15*-null, with no regions indicating increased c-Fos expression (Figs. 4c and d). Interestingly, within the amygdala, including the central amygdalar nucleus and basolateral amygdalar nucleus, c-Fos expression was consistently impaired during both ZT13 and ZT7. Moreover, decreased c-Fos expression was observed in the hypothalamus, an important center for thermoregulation, of *Pcdh15*-null during ZT7.

### DISCUSSION

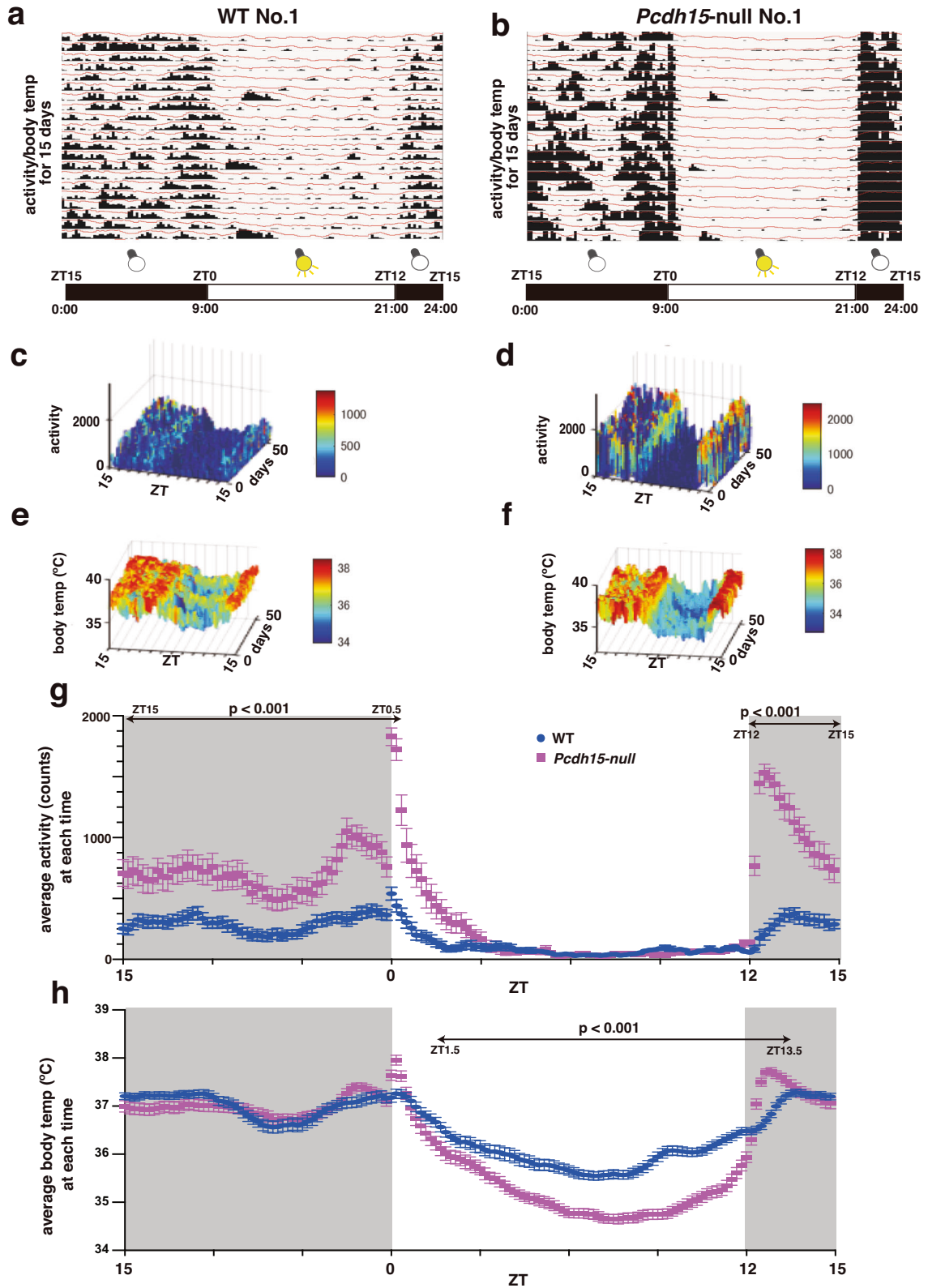
In this study, we demonstrated that *Pcdh15*-deletion mice display traits consistent with construct and surface validities, rendering them reliable models for the investigation of psychiatric disorders such as BD. The conclusions are based on observable phenotypic characteristics, such as hyperactivity, decreased PPI, and increased impulsivity, in these mice. The regulation of body temperature is a core biological function affected by circadian rhythms. However, this is known to be disturbed in BD [36] and the expected dysregulation was observed. Our extensive nano tag measurements over a prolonged period revealed a significant diurnal variation in body temperature in the *Pcdh15*-deletion mice. We further elucidated the neural mechanisms underlying these phenotypic traits by performing comprehensive c-Fos mapping across the entire brain.

### *Pcdh15*-deletion model mice compared with *av* mice: model of Usher syndrome

Via a whole-genome analysis targeting Japanese patients with psychiatric disorders, such as BD, we identified multiple patients with a loss of the protein-coating-encoding region of the *PCDH15* gene [4]. According to various databases, such as UniProt, the *PCDH15* gene exhibits diverse isoforms. Three types of intracellular domains, CD1, CD2, and CD3, are well known on the C-terminal end of the protein product. Furthermore, the cell-guidance domain located on the N-terminal side is highly diverse. Therefore, rather than mimicking specific patients, we aimed to focus on exons encoding a greater number of proteins reported in the database, and aimed to nullify *PCDH15*. Particularly, the CD3 isoform (UniProt: Q99PJ1-18) is abundantly expressed in the brain. Exon 5 of Q99PJ1-18 has a length of 161 bp, which is not a multiple of three, and it was selected because a suitable guide RNA for CRISPR/Cas9 cleavage could be designed.

Usher syndrome type 1 (USH1) is a genetic disorder that is characterized by severe hearing loss and retinitis pigmentosa [36]; furthermore, variants in the *Pcdh15* gene have been identified in families with Usher syndrome type 1F (USH1F) [11]. The mouse Ames waltzer hearing-loss mutant (*av*) exhibits a phenotype associated with hearing loss and balance disorders caused by degeneration of the inner ear neuroepithelium, with the *Pcdh15* gene being identified as the causative gene of this condition [37]. RT-PCR results showed that the *av* mutant mice *av-1*, *av-2J*, and *av-3J* are all incapable of expressing the full-length PCDH15 protein [37]. Similarly, our novel *Pcdh15*-deletion mice did not express the full-length PCDH15 protein, as confirmed via immunoblot analysis (Fig. 1d), thus sharing a commonality with the *av* mice.

*PCDH15* gene expression is restricted to the brain and inner ear [37]. Our *Pcdh15*-null mice did not exhibit lethality. *Pcdh15*<sup>av-2J</sup>



mice carry a spontaneous mutation at the *Pcdh15* locus and are characterized by head tossing, circling, and deafness [37]. Severe head tossing and circling were also observed in our *Pcdh15*-null mice (Fig. S2, Movie S1). PCDH15 expression has been identified by immunostaining the stereocilia of cochlear hair cells and retinal

photoreceptors, which are presumed to be necessary for their formation and maintenance [32]. It was anticipated that the loss of PCDH15 would result in fatal structural abnormalities in the inner ears and retinas of *Pcdh15*-deficient mice. However, no such macroscopic structural abnormalities were observed in either the

**Fig. 3 Long-term activity and body temperature measurement with a miniature accelerometer: nano tag.** **a, b** The presented data spans the light–dark (L–D) cycle of a mouse model, where the nano tag was intraperitoneally implanted and visualized through the nano tag Viewer software. Data for the first 15 days are displayed. The horizontal axis represents the time from ZT15 (00:00) to ZT15 (00:00) of the following day. The vertical axis histograms indicate activity levels per 5 min, whereas the line graphs depict body temperature. **a** represents WT No. 1 and **b** represents *Pcdh15*-null No. 1. Data for the other WT and *Pcdh15*-null (No. 2, 3, and 4) are shown in Supplementary Figure 4. **c–f** Three-dimensional surface plots created using MATLAB software (The MathWorks Inc., Natick, Massachusetts, USA) illustrate the activity and temperature fluctuations across time for the entire monitoring period. The color bars denote the intensity of each parameter: **c** activity in WT; **d** activity in *Pcdh15*-null; **e** body temperature in WT; and **f** body temperature in *Pcdh15*-null. **g, h** Mean  $\pm$  SEM of 6-week data obtained from four WT and four *Pcdh15*-null; the data were measured throughout the L–D cycle and plotted against time. The vertical axis represents activity (**g**) or body temperature (**h**) in 10-min intervals, whereas the horizontal axis depicts time within a 24-h period. A statistical analysis of the activity levels or body temperature at each time point was conducted via multiple *t*-tests using the GraphPad Prism 8 software, indicating significant time intervals with  $P < 0.001$ . In terms of activity levels, *Pcdh15*-null mice exhibited increased activity compared with the controls at all time points from lights off until 30 min after the lights were turned back on. Regarding body temperature, significant differences were observed at all time points from 1 h 30 min after lights on to 1 h 30 min after lights off. ZT Zeitgeber time.

inner ears or retinas of the *Pcdh15*-deficient mouse model (Fig. 1c and d). Thus, there may be a need to investigate more-subtle structural and functional abnormalities.

The cause of the phenotypic differences observed between *Pcdh15*-deficient mice and the *av* lines is unknown; however, they may be attributed to variations in the cleavage of the PCDH15 protein/mRNA product. Using immunoblotting, we confirmed the complete loss of the full-length PCDH15 protein (Fig. 1b, S1d). The PCDH15 signal is also lost in the immunostaining of *av* mice [38]. Higher organisms, including mice, exhibit a wide array of alternative splicing isoforms in both the extracellular and intracellular regions of the *Pcdh15* gene; hence, disparities in the impact of incomplete gene products caused by disrupted exons may arise.

#### Validity of *Pcdh15*-deletion mice as a psychiatric model

Historically, most studies on animal models of psychiatric disorders began by identifying animal behaviors mirroring human pathology, focusing primarily on surface validity. Subsequent studies explored predictive and construct validities [39]. However, models involving rare CNVs that are generally associated with a high risk of psychiatric disorders have recently emerged [40, 41]. Notably, these models have distinctly prioritized the establishment of construct validity from the outset. Similarly, we attempted to create a mouse model of psychiatric disease that meets the criteria for construct validity. This was accomplished through the targeted deletion of *Pcdh15*, a gene recognized in patients with psychiatric disorders. Subsequently, we evaluated the surface validity of this model. Our findings indicate that *Pcdh15*-deletion mice display phenotypes consistent with those observed in analogous disease models [42–45] and patients [46–50]. Consequently, *Pcdh15*-deletion mice appear to be a promising model for psychiatric disorders, satisfying both construct and face validity criteria.

We have previously highlighted the significant association of *Pcdh15* deletion with BD [4]. Certain phenotypes, such as the hyperactivity noted in *Pcdh15*-deletion mice, may mirror the manic symptoms of BD. Whole-brain c-Fos mapping has shown altered neural activity in the amygdala, a region where structural abnormalities frequently occur in adult patients with BD or SCZ [51–53]. The consistent dysfunction of the amygdala implies that *Pcdh15*-deletion mice may also satisfy surface validity as a model of psychiatric disorders in terms of brain function.

Throughout 6 weeks of extended observations using nano tags, *Pcdh15*-null consistently displayed manic (hyperlocomotive) behavior rather than depressive (hypolocomotive) tendencies. A comparison can be drawn with the mitochondrial DNA polymerase catalytic subunit (*Polg1*) mutant mice, a model for BD, where multiple episodes of inactivity were detected over a 6-month observation period [54]. To enhance the face validity of *Pcdh15*-deletion mice in modeling BD, extending the observational period

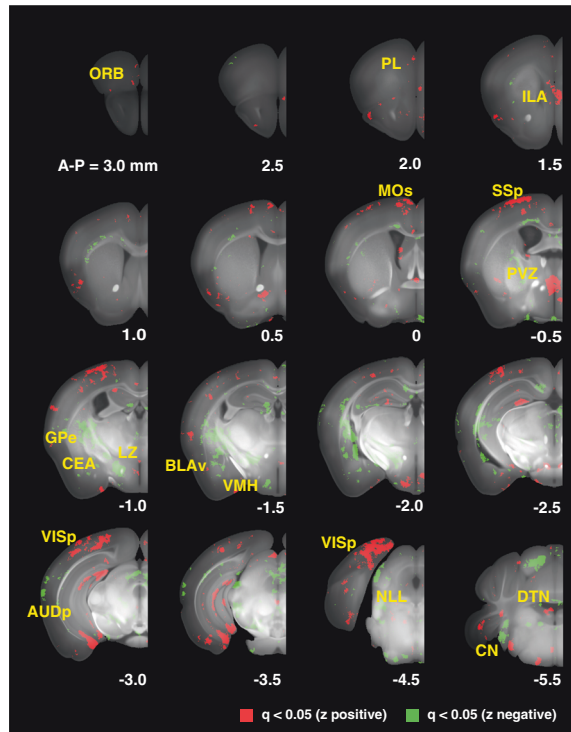
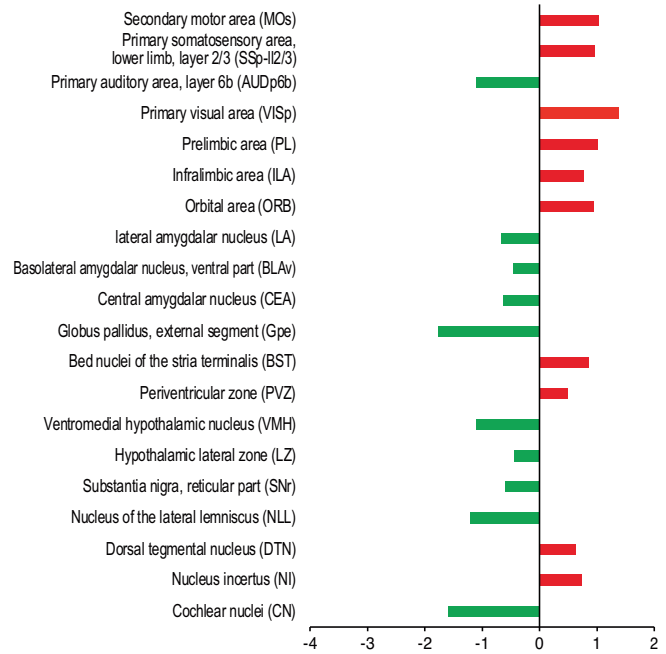
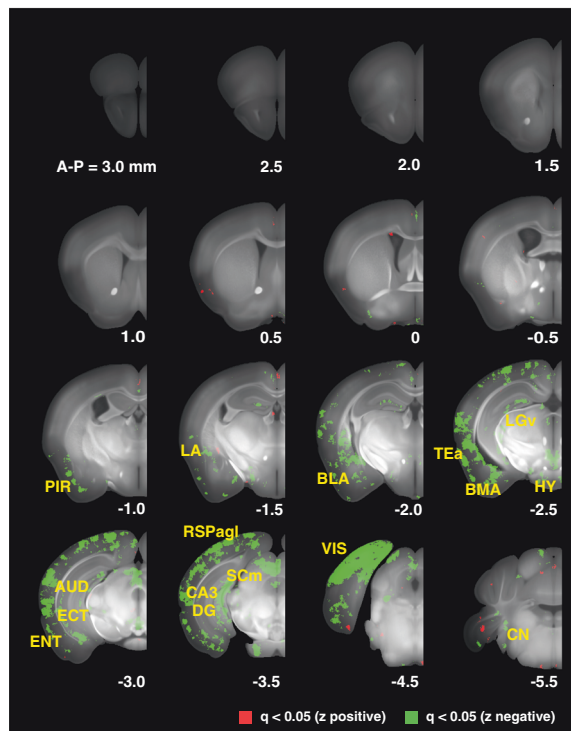
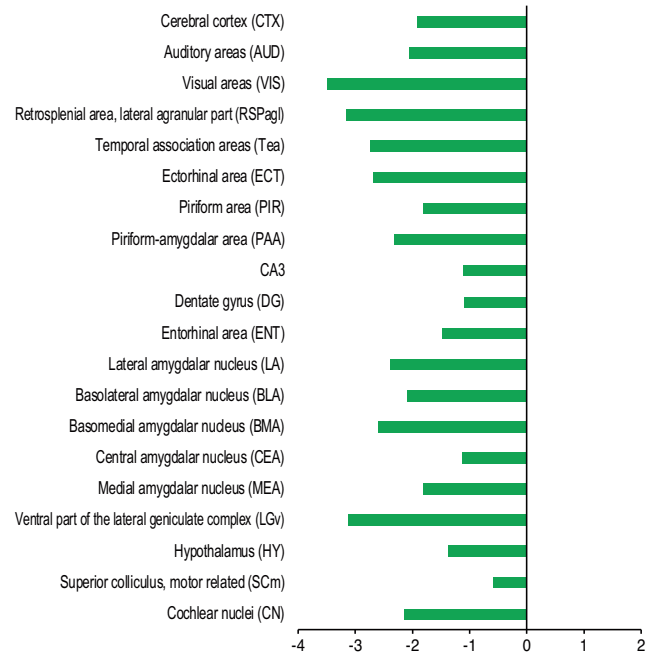
using nano tags might help capture both manic and depressive episodes, thereby characterizing the cyclical nature of BD.

#### Phenotypes of *Pcdh15*-deletion mice

BD, which is genetically linked to *PCDH15* deletion, manifests as recurring depressive and manic episodes [55]. Manic episodes are marked by symptoms such as euphoria, aggression, sleep disruptions, elevated reward-seeking behavior, hypersexuality, and hyperactivity [56, 57]. Our tests revealed *Pcdh15*-het displayed hyperactivity (Fig. 2a), diminished PPI (Fig. 2b), and increased impulsivity (Fig. 2c). These findings mirror those of previously documented mouse models of mania [42, 44] and patients with BD [48–50]. Some overlapping phenotypes have been observed in patients with ASD and SCZ or animal models with *Pcdh15* deletion [43, 45–47].

However, behavioral tests can be skewed by various external factors, such as the testing environment or researcher [58, 59]. The behavior of mice outside the home cage or when isolated can be erratic. The importance of conducting long-term behavioral observations in a less constrained and more natural environment has also been recognized [60]. In our analysis, we employed the nano tag system to address these issues [61, 62]. Despite its significant weight in relation to the mice, the nano tag successfully highlighted the hyperactive tendencies in *Pcdh15*-null across 6 weeks in their home cages. We demonstrated similar results on a 24-h continuous locomotor activity test by assessing activity based on the number of crossings of an infrared beam (Fig. S3). The hyperlocomotive behavior of *Pcdh15*-null was more pronounced immediately after light-off and subdued after light-on (Fig. 3 and S4). Patients with psychiatric disorders, including BD, often suffer from sleep disturbances, including circadian rhythm disruptions [63]. However, *Pcdh15*-null mice did not exhibit significant circadian rhythm abnormalities (Fig. S5a). Despite the increased activity levels, their daily rest hours were not significantly different from those of WT (Figs. S5b and S5c). While activity-based sleep–wake rhythm analysis is common in rotating cages [64], comprehensive studies integrating electroencephalography and other methodologies are required to fully understand the effect of *Pcdh15* deletion on sleep.

Another key feature of the nano tag is its ability to measure core body temperature. In our study, *Pcdh15*-null exhibited their lowest body temperature around ZT7 during the light-on period. The values peaked at ZT13 after light-off (Fig. 3h). *Pcdh15*-null showed a diurnal temperature amplitude that was 1.7 times greater than that of WT. The hypothalamus acts as the thermoregulatory center of the brain [65]. The periventricular zone, which showed increased c-Fos expression at ZT13 in *Pcdh15*-null, is a hypothalamic region containing the paraventricular hypothalamic nucleus, which is part of a neural circuit essential for emotion and thermoregulation [66]. The temperature increase toward ZT13 may be attributed to the activation of the paraventricular hypothalamic nucleus. Conversely, at ZT7, *Pcdh15*-null exhibited

**a** *Pcdh15*-null vs WT at ZT13 (light-off)**b**log<sub>2</sub> fold change of cell count at ZT13**c** *Pcdh15*-null vs WT at ZT7 (light-on)**d**log<sub>2</sub> fold change of cell count at ZT7

**Fig. 4** **c-Fos mapping in the *Pcdh15*-null whole brain.** **a–d** Results of automated analysis of c-Fos-positive cell distribution in mouse brains collected at ZT13 or ZT7.  $n = 3$  for WT and  $n = 3$  for *Pcdh15*-null.  $q$  value voxel maps comparing WT with *Pcdh15*-null (**a**) at ZT13 and (**c**) at ZT7. A-P: distance from bregma in mm. Bar plots illustrating the log<sub>2</sub> fold-change in each brain region (**b**) at ZT13 and (**d**) at ZT7. Red voxels and bars indicate  $q < 0.05$  and  $z > 0$ . Green voxels and bars indicate  $q < 0.05$  and  $z < 0$ .



reduced c-Fos expression in the hypothalamus, which includes the dorsomedial nucleus of the hypothalamus ( $q = 5.37 \times 10^{-9}$ ), a vital component of the previously mentioned neural circuit. The exact mechanism responsible for the fluctuations in temperature due to *Pcdh15* deletion remains elusive. Hence, there is a need for a thorough examination of the interplay between the hypothalamic regions and metabolism.

### Relationships between phenotypes and brain activity in *Pcdh15*-null

c-Fos is a transcription factor robustly induced by neural activity, with expression peaking within 5–10 min of stimulation and lasting 2–3 h [67–69]. Consequently, it serves as a reliable marker of recent neural activity [68, 70].

In this investigation, c-Fos mapping illuminated the brain activity landscape in *Pcdh15*-null. At ZT13, *Pcdh15*-null brains exhibited increased c-Fos expression in the primary visual cortex, prefrontal cortex, and orbital regions compared with those of WT. In contrast, they showed decreased levels in the amygdala, globus pallidus, and certain hypothalamic regions (Fig. 4a and b). However, at ZT7, numerous regions in *Pcdh15*-null brains showed reduced c-Fos expression (Figs. 4c and d). Notably, *Pcdh15*-null brains at both ZT7 and ZT13 were characterized by decreased c-Fos levels in the amygdala, a pivotal region for emotions such as fear and anxiety [71]. This reduced activity could mirror emotional and interpersonal deficits observed in psychiatric disorders [72]. Based on magnetic resonance imaging findings suggesting a structurally reduced amygdala in BD and SCZ [51–53], a more comprehensive exploration of this aspect in *Pcdh15*-null is warranted. The Yakovlev circuit is centered in the amygdala and links the orbitofrontal cortex, insula, and anterior temporal lobe; it underpins emotions and motivation [73, 74]. In *Pcdh15*-null at ZT13, alterations in c-Fos expression were observed in multiple brain regions encompassed by this circuit, extending beyond the amygdala. This suggests that disruptions in this circuitry could potentially contribute to the manifestation of symptoms related to psychiatric diseases.

Correlating c-Fos mapping to observed phenotypes, c-Fos expression was elevated at ZT13 (the active phase) in both WT and *Pcdh15*-null compared with that at ZT7 (Fig. S6b). This surge in the hyperlocomotive *Pcdh15*-null at ZT13 may be ascribed to increased physical activity [75]. This hypothesis aligns with findings indicating that running elevates c-Fos in areas such as the primary somatosensory and secondary motor cortex [76].

*Pcdh15* deletion has also been linked to diminished PPI (Fig. 2b). While the neural circuits governing PPI have been identified [77], it is established that inhibition of the globus pallidus dampens PPI [78]. In our study, the globus pallidus in *Pcdh15*-null at ZT13 showed reduced c-Fos expression. The auditory cortex, another PPI player [79], exhibited decreased c-Fos levels in *Pcdh15*-null at ZT13.

Furthermore, *Pcdh15* deletion correlated with increased impulsivity (Fig. 2c). The orbitofrontal cortex is implicated in impulsivity [80] and structurally altered in patients with BD [81]. It interacts with the amygdala, thereby suppressing its activity [82]. This interplay in *Pcdh15*-null at ZT13 potentially underlies the increased impulsivity and other psychiatric symptoms.

Comparison of WT and mutant mice under consistent conditions revealed variations in c-Fos expression across brain regions. Immunostaining of the primary visual cortex confirmed our c-Fos mapping findings (Fig. S6c). Furthermore, analysis of samples obtained from around this cortex through reverse transcription-polymerase chain reaction revealed congruent c-Fos mRNA levels (Figs. S6d and e). These findings affirm the utility of c-Fos brain mapping for analyzing neural activity in mutant mice and considering the neural circuit basis of the phenotype.

This study had some limitations. First, this model lacks validation regarding the predictive validity of BD. Second, the effects of treatment using existing therapeutic agents on the activity and body temperature need to be investigated. In the future, as more comprehensive genomic analysis data of patients with psychiatric disorders, including BD, becomes available, there is a sufficient possibility that the genetic association between the *PCDH15* variants and onset could become statistically significant from a genetic standpoint.

In conclusion, the results of our study revealed that *Pcdh15*-deletion mice display key phenotypes, including hyperactivity. Our comprehensive analysis of whole-brain activity provided significant insights into the neural circuitry underlying these phenotypes. Considering these findings, *Pcdh15*-deletion mice emerge as a potentially valuable model, meeting both construct and surface validity criteria, for investigating the mechanisms linking *PCDH15* deletion to psychiatric disorders, notably BD with mania.

### DATA AVAILABILITY

The datasets generated during and/or analyzed during the current study are available from the corresponding author upon reasonable request.

### REFERENCES

- Andreassen OA, Hindley GFL, Frei O, Smeland OB. New insights from the last decade of research in psychiatric genetics: discoveries, challenges and clinical implications. *World Psychiatry*. 2023;22:4–24.
- Georgieva L, Rees E, Moran JL, Chambert KD, Milanova V, Craddock N, et al. De novo CNVs in bipolar affective disorder and schizophrenia. *Hum Mol Genet*. 2014;23:6677–83.
- Noor A, Lionel AC, Cohen-Woods S, Moghimi N, Rucker J, Fennell A, et al. Copy number variant study of bipolar disorder in Canadian and UK populations implicates synaptic genes. *Am J Med Genet B Neuropsychiatr Genet*. 2014;165B:303–13.
- Kushima I, Nakatochi M, Aleksic B, Okada T, Kimura H, Kato H, et al. Cross-disorder analysis of genetic and regulatory copy number variations in bipolar disorder, schizophrenia, and autism spectrum disorder. *Biol Psychiatry*. 2022;92:362–74.
- Sotomayor M, Weihofen WA, Gaudet R, Corey DP. Structure of a force-conveying cadherin bond essential for inner-ear mechanotransduction. *Nature*. 2012;492:128–32.
- Hirano S, Takeichi M. Cadherins in brain morphogenesis and wiring. *Physiol Rev*. 2012;92:597–634.
- Franke B, Neale BM, Faraone SV. Genome-wide association studies in ADHD. *Hum Genet*. 2009;126:13–50.
- Balan S, Ohnishi T, Watanabe A, Ohba H, Iwayama Y, Toyoshima M, et al. Role of an Atypical Cadherin Gene, *Cdh23* in prepulse inhibition, and implication of *CDH23* in Schizophrenia. *Schizophr Bull*. 2021;47:1190–1200.
- Ishii T, Ishikawa M, Fujimori K, Maeda T, Kushima I, Arioka Y, et al. In vitro modeling of the bipolar disorder and schizophrenia using patient-derived induced pluripotent stem cells with copy number variations of *PCDH15* and *RELN*. *eNeuro* 2019; 6.
- Huang W, Bhaduri A, Velmeshev D, Wang S, Wang L, Rottkamp CA, et al. Origins and proliferative states of human oligodendrocyte precursor cells. *Cell*. 2020;182:594–608.e511.
- Ahmed ZM, Riazuddin S, Bernstein SL, Ahmed Z, Khan S, Griffith AJ, et al. Mutations of the protocadherin gene *PCDH15* cause Usher syndrome type 1F. *Am J Hum Genet*. 2001;69:25–34.
- Yoshimura H, Miyagawa M, Kumakawa K, Nishio SY, Usami S. Frequency of Usher syndrome type 1 in deaf children by massively parallel DNA sequencing. *J Hum Genet*. 2016;61:419–22.
- Sethna S, Zein WM, Riaz S, Giese AP, Schultz JM, Duncan T, et al. Proposed therapy, developed in a *Pcdh15*-deficient mouse, for progressive loss of vision in human Usher syndrome. *Elife*. 2021;10:e67361.
- Rao NP, Danivas V, Venkatasubramanian G, Behere RV, Gangadhar BN. Comorbid bipolar disorder and Usher syndrome. *Prim Care Companion J Clin Psychiatry*. 2010;12:PCC.09I00792.
- Domanico D, Fragiotta S, Cutini A, Grenga PL, Vingolo EM. Psychosis, mood and behavioral disorders in usher syndrome: review of the literature. *Med Hypothesis Discov Innov Ophthalmol*. 2015;4:50–55.
- Belzung C, Lemoine M. Criteria of validity for animal models of psychiatric disorders: focus on anxiety disorders and depression. *Biol Mood Anxiety Disord*. 2011;1:9.

17. Willner P. Validation criteria for animal models of human mental disorders: learned helplessness as a paradigm case. *Prog Neuropsychopharmacol Biol Psychiatry*. 1986;10:677–90.
18. Willner P. The validity of animal models of depression. *Psychopharmacology (Berl)*. 1984;83:1–16.
19. McCarty R, Josephs T, Kovtun O, Rosenthal SJ. Correction: Enlightened: addressing circadian and seasonal changes in photoperiod in animal models of bipolar disorder. *Transl Psychiatry*. 2021;11:400.
20. Beyer DKE, Freund N. Animal models for bipolar disorder: from bedside to the cage. *Int J Bipolar Disord*. 2017;5:35.
21. Sharma AN, Fries GR, Galvez JF, Valvassori SS, Soares JC, Carvalho AF, Quevedo J. Modeling mania in preclinical settings: A comprehensive review. *Prog Neuropsychopharmacol Biol Psychiatry*. 2016;66:22–34.
22. Malkesman O, Austin DR, Chen G, Manji HK. Reverse translational strategies for developing animal models of bipolar disorder. *Dis Model Mech*. 2009;2:238–45.
23. Mori D, Ikeda R, Sawahata M, Yamaguchi S, Kodama A, Hirao T, et al. Phenotypes for general behavior, activity, and body temperature in 3q29 deletion model mice. *Transl Psychiatry*. 2024;14:138.
24. Sekiguchi M, Sobue A, Kushima I, Wang C, Arioka Y, Kato H, et al. ARHGAP10, which encodes Rho GTPase-activating protein 10, is a novel gene for schizophrenia risk. *Transl Psychiatry*. 2020;10:247.
25. Sawahata M, Mori D, Arioka Y, Kubo H, Kushima I, Kitagawa K, et al. Generation and analysis of novel Reln-deleted mouse model corresponding to exonic Reln deletion in schizophrenia. *Psychiatry Clin Neurosci*. 2020;74:318–27.
26. Aida T, Chiyo K, Usami T, Ishikubo H, Imahashi R, Wada Y, et al. Cloning-free CRISPR/Cas system facilitates functional cassette knock-in in mice. *Genome Biol*. 2015;16:87.
27. Urata S, Iida T, Yamamoto M, Mizushima Y, Fujimoto C, Matsumoto Y, et al. Cellular cartography of the organ of Corti based on optical tissue clearing and machine learning. *Elife*. 2019;8:e40946.
28. Nishiguchi KM, Carvalho LS, Rizzi M, Powell K, Holthaus SM, Azam SA, et al. Gene therapy restores vision in rd1 mice after removal of a confounding mutation in Gpr179. *Nat Commun*. 2015;6:6006.
29. Kuroda K, Yamada S, Tanaka M, Iizuka M, Yano H, Mori D, et al. Behavioral alterations associated with targeted disruption of exons 2 and 3 of the Disc1 gene in the mouse. *Hum Mol Genet*. 2011;20:4666–83.
30. Renier N, Adams EL, Kirst C, Wu Z, Azevedo R, Kohl J, et al. Mapping of brain activity by automated volume analysis of immediate early genes. *Cell*. 2016;165:1789–802.
31. Ahmed ZM, Riazuddin S, Aye S, Ali RA, Venselaar H, Anwar S, et al. Gene structure and mutant alleles of PCDH15: nonsyndromic deafness DFNB23 and type 1 Usher syndrome. *Hum Genet*. 2008;124:215–23.
32. Ahmed ZM, Riazuddin S, Ahmad J, Bernstein SL, Guo Y, Sabar MF, et al. PCDH15 is expressed in the neurosensory epithelium of the eye and ear and mutant alleles are responsible for both USH1F and DFNB23. *Hum Mol Genet*. 2003;12:3215–23.
33. Sagar SM, Sharp FR, Curran T. Expression of c-fos protein in brain: metabolic mapping at the cellular level. *Science*. 1988;240:1328–31.
34. Procaccini C, Aitta-aho T, Jaako-Movits K, Zharkovsky A, Panhelainen A, Sprengel R, et al. Excessive novelty-induced c-Fos expression and altered neurogenesis in the hippocampus of GluA1 knockout mice. *Eur J Neurosci*. 2011;33:161–74.
35. Ueda HR, Dödt HU, Osten P, Economo MN, Chandrasekar J, Keller PJ. Whole-brain profiling of cells and circuits in mammals by tissue clearing and light-sheet microscopy. *Neuron*. 2020;106:369–87.
36. Smith RJ, Berlin CI, Hejtmancik JF, Keats BJ, Kimberling WJ, Lewis RA, et al. Clinical diagnosis of the Usher syndromes. Usher Syndrome Consortium. *Am J Med Genet*. 1994;50:32–38.
37. Alagramam KN, Murcia CL, Kwon HY, Pawlowski KS, Wright CG, Woychik RP. The mouse Ames waltzer hearing-loss mutant is caused by mutation of Pcdh15, a novel protocadherin gene. *Nat Genet*. 2001;27:99–102.
38. Senften M, Schwander M, Kazmierczak P, Lillo C, Shin JB, Hasson T, et al. Physical and functional interaction between protocadherin 15 and myosin VIIa in mechanosensory hair cells. *J Neurosci*. 2006;26:2060–71.
39. Einat H, Belmaker RH, Manji HK. New approaches to modeling bipolar disorder. *Psychopharmacol Bull*. 2003;37:47–63.
40. Forrest MP, Penzes P. Mechanisms of copy number variants in neuropsychiatric disorders: From genes to therapeutics. *Curr Opin Neurobiol*. 2023;82:102750.
41. Forsingdal A, Jorgensen TN, Olsen L, Werge T, Didriksen M, Nielsen J. Can animal models of copy number variants that predispose to schizophrenia elucidate underlying biology? *Biol Psychiatry*. 2019;85:13–24.
42. Kristensen M, Nierenberg AA, Ostergaard SD. Face and predictive validity of the ClockDelta19 mouse as an animal model for bipolar disorder: a systematic review. *Mol Psychiatry*. 2018;23:70–80.
43. Jhang CL, Huang TN, Hsueh YP, Liao W. Mice lacking cyclin-dependent kinase-5 manifest autistic and ADHD-like behaviors. *Hum Mol Genet*. 2017;26:3922–34.
44. van Enkhuizen J, Minassian A, Young JW. Further evidence for ClockDelta19 mice as a model for bipolar disorder mania using cross-species tests of exploration and sensorimotor gating. *Behav Brain Res*. 2013;249:44–54.
45. Fabricius K, Helboe L, Fink-Jensen A, Wortwein G, Steiniger-Brach B. Pharmacological characterization of social isolation-induced hyperactivity. *Psychopharmacology*. 2011;215:257–66.
46. Li S, Lu C, Kang L, Li Q, Chen H, Zhang H, et al. Study on correlations of BDNF, PI3K, AKT and CREB levels with depressive emotion and impulsive behaviors in drug-naive patients with first-episode schizophrenia. *BMC Psychiatry*. 2023;23:225.
47. Zhang J, Wang M, Wei B, Shi J, Yu T. Research progress in the study of startle reflex to disease states. *Neuropsychiatr Dis Treat*. 2022;18:427–35.
48. Mao Z, Bo Q, Li W, Wang Z, Ma X, Wang C. Prepulse inhibition in patients with bipolar disorder: a systematic review and meta-analysis. *BMC Psychiatry*. 2019;19:282.
49. Wingo AP, Ghaemi SN. A systematic review of rates and diagnostic validity of comorbid adult attention-deficit/hyperactivity disorder and bipolar disorder. *J Clin Psychiatry*. 2007;68:1776–84.
50. Najt P, Perez J, Sanches M, Peluso MA, Glahn D, Soares JC. Impulsivity and bipolar disorder. *Eur Neuropsychopharmacol*. 2007;17:313–20.
51. Barth C, Nerland S, de Lange AG, Wortinger LA, Hilland E, Andreassen OA, et al. In Vivo Amygdala nuclei volumes in schizophrenia and bipolar disorders. *Schizophr Bull*. 2021;47:1431–41.
52. Okada N, Fukunaga M, Yamashita F, Koshiyama D, Yamamori H, Ohi K, et al. Abnormal asymmetries in subcortical brain volume in schizophrenia. *Mol Psychiatry*. 2016;21:1460–6.
53. Phillips ML, Swartz HA. A critical appraisal of neuroimaging studies of bipolar disorder: toward a new conceptualization of underlying neural circuitry and a road map for future research. *Am J Psychiatry*. 2014;171:829–43.
54. Kasahara T, Takata A, Kato TM, Kubota-Sakashita M, Sawada T, Kakita A, et al. Depression-like episodes in mice harboring mtDNA deletions in paraventricular thalamus. *Mol Psychiatry*. 2016;21:39–48.
55. Association, AP. APA releases diagnostic and statistical manual of mental disorders, fifth edition, text revision (DSM-5-TR). <https://www.psychiatry.org/newsroom/news-releases/apa-releases-diagnostic-and-statistical-manual-of-mental-disorders-fifth-edition-text-revision-dsm-5-tr> Date: March 18, 2022, Date accessed: April 20, 2022 2022.
56. Cheniaux E, Filgueiras A, Silva Rde A, Silveira LA, Nunes AL, Landeira-Fernandez J. Increased energy/activity, not mood changes, is the core feature of mania. *J Affect Disord*. 2014;152-154:256–61.
57. Perry W, Minassian A, Henry B, Kincaid M, Young JW, Geyer MA. Quantifying over-activity in bipolar and schizophrenia patients in a human open field paradigm. *Psychiatry Res*. 2010;178:84–91.
58. Crabbe JC, Wahlsten D, Dudek BC. Genetics of mouse behavior: interactions with laboratory environment. *Science*. 1999;284:1670–2.
59. Segelcke D, Talbot SR, Palme R, La Porta C, Pogatzki-Zahn E, Bleich A, Tappe-Theodor A. Experimenter familiarization is a crucial prerequisite for assessing behavioral outcomes and reduces stress in mice not only under chronic pain conditions. *Sci Rep*. 2023;13:2289.
60. Smith K. Lab mice go wild: making experiments more natural in order to decode the brain. *Nature*. 2023;618:448–50.
61. Funabashi D, Wakiyama Y, Muto N, Kita I, Nishijima T. Social isolation is a direct determinant of decreased home-cage activity in mice: A within-subjects study using a body-implantable actimeter. *Exp Physiol*. 2022;107:133–46.
62. Sakai K, Ishikawa A, Mizuno Y, Maki T, Oda Y, Takahashi E. Simplified drug efficacy screening system for sleep-disorder drugs using non-human primates. *Heliyon*. 2020;6:e03524.
63. Harvey AG. Sleep and circadian rhythms in bipolar disorder: seeking synchrony, harmony, and regulation. *Am J Psychiatry*. 2008;165:820–9.
64. Bains RS, Wells S, Sillito RR, Armstrong JD, Cater HL, Banks G, Nolan PM. Assessing mouse behaviour throughout the light/dark cycle using automated in-cage analysis tools. *J Neurosci Methods*. 2018;300:37–47.
65. Morrison SF, Nakamura K. Central neural pathways for thermoregulation. *Front Biosci (Landmark Ed)*. 2011;16:74–104.
66. Nakamura K. Neural circuit for psychological stress-induced hyperthermia. *Temperature*. 2015;2:352–61.
67. Senba E, Ueyama T. Stress-induced expression of immediate early genes in the brain and peripheral organs of the rat. *Neurosci Res*. 1997;29:183–207.
68. Morgan JI, Cohen DR, Hempstead JL, Curran T. Mapping patterns of c-fos expression in the central nervous system after seizure. *Science*. 1987;237:192–7.
69. Greenberg ME, Ziff EB, Greene LA. Stimulation of neuronal acetylcholine receptors induces rapid gene transcription. *Science*. 1986;234:80–83.
70. Cho JH, Rendall SD, Gray JM. Brain-wide maps of Fos expression during fear learning and recall. *Learn Mem*. 2017;24:169–81.
71. LeDoux JE. Emotion circuits in the brain. *Annu Rev Neurosci*. 2000;23:155–84.

72. Decety J, Moriguchi Y. The empathic brain and its dysfunction in psychiatric populations: implications for intervention across different clinical conditions. *Biopsychosoc Med.* 2007;1:22.
73. Yakovlev PI. Motility, behavior and the brain; stereodynamic organization and neural coordinates of behavior. *J Nerv Ment Dis.* 1948;107:313–35.
74. Catani M, Dell'acqua F, Thiebaut de Schotten M. A revised limbic system model for memory, emotion and behaviour. *Neurosci Biobehav Rev.* 2013;37:1724–37.
75. Robins MT, Li J, Ryabinin AE. Effects of housing conditions and circadian time on baseline c-Fos immunoreactivity in C57BL/6J Mice. *Neuroscience.* 2020;431:143–51.
76. Tsai SF, Liu YW, Kuo YM. Acute and long-term treadmill running differentially induce c-Fos expression in region- and time-dependent manners in mouse brain. *Brain Struct Funct.* 2019;224:2677–89.
77. Niu H, He X, Zhou T, Shi X, Zhang Q, Zhang Z, et al. Neural circuits containing olfactory neurons are involved in the prepulse inhibition of the startle reflex in rats. *Front Behav Neurosci.* 2015;9:74.
78. Takahashi K, Nagai T, Kamei H, Maeda K, Matsuya T, Arai S, et al. Neural circuits containing pallidotegmental GABAergic neurons are involved in the prepulse inhibition of the startle reflex in mice. *Biol Psychiatry.* 2007;62:148–57.
79. Moyer CE, Erickson SL, Fish KN, Thiels E, Penzes P, Sweet RA. Developmental trajectories of auditory cortex synaptic structures and gap-prepulse inhibition of acoustic startle between early adolescence and young adulthood in mice. *Cereb Cortex.* 2016;26:2115–26.
80. Zeeb FD, Floresco SB, Winstanley CA. Contributions of the orbitofrontal cortex to impulsive choice: interactions with basal levels of impulsivity, dopamine signaling, and reward-related cues. *Psychopharmacology.* 2010;211:87–98.
81. Nery FG, Chen HH, Hatch JP, Nicoletti MA, Brambilla P, Sassi RB, et al. Orbitofrontal cortex gray matter volumes in bipolar disorder patients: a region-of-interest MRI study. *Bipolar Disord.* 2009;11:145–53.
82. Chang CH, Grace AA. Inhibitory modulation of Orbitofrontal cortex on medial prefrontal cortex-amygdala information flow. *Cereb Cortex.* 2018;28:1–8.

## ACKNOWLEDGEMENTS

We thank all the members for participating in this study; Division of Experimental Animals and Division for Medical Research Engineering, Nagoya University Graduate School of Medicine for their technical support. We are indebted to Kazuhiro Nakamura and Manami Oya for helpful discussions. We appreciate the valuable assistance provided by ChatGPT in enhancing the quality of the English language. We would like to thank Enago Editing Service (Japan) for professional English proofreading and editing of the manuscript. Funding for this study was provided by research grants from the Ministry of Education, Culture, Sports, Science and Technology of Japan; the Ministry of Health, Labor and Welfare of Japan; and AMED under grant No. JP21wm0425007, JP19dm0207075, JP19dm0207069, JP21dk0307103, JP20ek0109488, JP20dk0307099, JP22tm0424222, JP22gm1410011, JP23gm1910005, JP23ek0109678, JP19ak0101126 and JP19ak0101113; and the Japan Society for the Promotion of Science (JSPS) KAKENHI

Grant No. 20K20602, 21H04815, 19K07384 and 22K07369; and Sumitomo Pharma Co., Ltd.

## AUTHOR CONTRIBUTIONS

DM and CI wrote the main text and prepared most of the figures; DM generated the *Pcdh15*-deletion mice; RI and MS performed most of the behavioral and histological experiments; DM performed nano tag assay; DM, CI, SY, and KK performed phase analysis; SU and SO performed histological analysis of inner ear; KN and KF performed histological analysis of retina; AK, YK, YA, HO, TS, AY, and TI performed molecular and cellular biological experiments; all other authors commented on and refined the manuscript; NO, KY, KK, KK, TN, HM, and YN supervised the overall project. All authors have carefully read the paper and approved the final manuscript.

## COMPETING INTERESTS

The authors declare no competing interests

## ADDITIONAL INFORMATION

**Supplementary information** The online version contains supplementary material available at <https://doi.org/10.1038/s41398-024-02952-6>.

**Correspondence** and requests for materials should be addressed to Daisuke Mori.

**Reprints and permission information** is available at <http://www.nature.com/reprints>

**Publisher's note** Springer Nature remains neutral with regard to jurisdictional claims in published maps and institutional affiliations.



**Open Access** This article is licensed under a Creative Commons Attribution 4.0 International License, which permits use, sharing, adaptation, distribution and reproduction in any medium or format, as long as you give appropriate credit to the original author(s) and the source, provide a link to the Creative Commons licence, and indicate if changes were made. The images or other third party material in this article are included in the article's Creative Commons licence, unless indicated otherwise in a credit line to the material. If material is not included in the article's Creative Commons licence and your intended use is not permitted by statutory regulation or exceeds the permitted use, you will need to obtain permission directly from the copyright holder. To view a copy of this licence, visit <http://creativecommons.org/licenses/by/4.0/>.

© The Author(s) 2024